

The effect of CO_3^{2-} on the growth of barite {001} and {210} surfaces: An AFM study

Nuria Sánchez-Pastor, Carlos M. Pina *, Lurdes Fernández-Díaz, José Manuel Astilleros

Dpto. Cristalografía y Mineralogía, Universidad Complutense de Madrid, C/ José Antonio Novais 2, E-28040 Madrid, Spain

Abstract

The growth of barite {001} and {210} faces from aqueous solutions moderately supersaturated with respect to barite ($\beta_{\text{barite}} \approx 12$ for experiments on {001} surfaces and $\beta_{\text{barite}} \approx 7$ for experiments on {210} surfaces) and bearing different concentrations of carbonate has been studied in situ using an atomic force microscope (AFM). Nanoscopic observations show that, above a certain carbonate concentration threshold in the aqueous solution, the advancement of monolayers (~ 3.5 Å in height) on barite {001} and {210} surfaces is strongly inhibited. However, inhibition never affects the growth of the first monolayer, whose growth rate increases in the presence of carbonate. In contrast, the second monolayer growth rate decreases as the concentration of carbonate in the solution increases. For high carbonate concentrations in the solution, growth stops after the formation of the first monolayer. While on barite {001} faces, the formation of a second monolayer does not occur for carbonate concentrations higher than 0.2 mM, on barite {210} faces the complete inhibition of the second monolayer is observed for carbonate concentrations higher than 0.05 mM. Once growth on {001} or {210} faces is completely inhibited, i.e. such surfaces are in the “dead zone”, growth can be recovered by increasing supersaturation. In order to study the recovery behaviour of barite {001} and {210} faces from the “dead zone”, an additional series of AFM experiments have been conducted. In these experiments, carbonate-free aqueous solutions with increasing supersaturations with respect to barite were passed over {001} and {210} surfaces previously “poisoned” with carbonate. Our experimental results show that the recovery of growth on barite {001} faces requires an important increase of the solution supersaturation. In contrast, the recovery of barite {210} surface growth does not require any supersaturation increase, but spontaneously occurs in a few minutes. Our observations of inhibition and growth recovery on barite surfaces at a nano-scale are discussed and compared with the descriptions given by the classical crystal growth inhibition models.

Keywords: Atomic force microscopy; Barite; Growth inhibition; Growth recovery

1. Introduction

Crystal growth inhibition is an interesting phenomenon that can be promoted by the presence of isomorphic impurities in the crystallization medium. The supersaturation conditions and impurity concentrations for which no growth is observed define the so-called “dead zone” [1–4].

Growth inhibition shows a progressive character, with crystal growth rate decreasing as impurity concentration increases in the growth medium. Finally, when impurity concentration reaches a certain value, growth completely stops. Growth inhibition phenomena associated with the presence of impurities in the growth medium differently affect different crystal faces, leading to the modification of crystal habit [5–7]. This effect has important implications both in biomineralization and in the preparation of technological materials, medical drugs, etc. Furthermore, crystal habit changes due to impurities can be used as clues in ore-deposits prospecting [6,8].

* Corresponding author. Tel.: +34 9139 44879;

E-mail addresses: nsanchez@geo.ucm.es (N. Sánchez-Pastor), cmpina@geo.ucm.es (C.M. Pina), lfdiaz@geo.ucm.es (L. Fernández-Díaz), jmastill@geo.ucm.es (J.M. Astilleros).

There are two main theoretical models which describe the kinetics of both inhibition and recovery of crystal growth: (i) the step-pinning model [1–3,9,10] and (ii) the isomorphic impurity incorporation model [11–13]. Both models have provided a satisfactory explanation for the macroscopic growth rates measured on crystals growing in the presence of organic and inorganic impurities, respectively [14, and references therein]. Nevertheless, the step-pinning model and the isomorphic impurity incorporation model interpret inhibition phenomenon assuming that different mechanisms operate at the nano-scale during growth of crystal surfaces. The first model proposes that inhibition occurs when large molecules block kink-sites. The second model assumes the incorporation of impurities in lattice positions, leading to the modification of the physical-chemistry properties of the growing crystal surface (mainly solubility) and promoting changes in the kinetics of growth units incorporation.

Although step-pinning and isomorphic impurity incorporation models represent a valuable description of crystal growth inhibition, recent AFM observations of crystal surfaces growing in the presence of impurities have shown that the nano-scale mechanisms of growth inhibition seem to be more complex than expected [4,15–20]. In particular, growth of the first monolayers from an “impure” aqueous solution on a pre-existing crystal face frequently shows an anomalous kinetics, which is difficult to explain only on the basis of the classic models. These results have made evident that understanding the ultimate mechanisms involved in crystal growth inhibition will require extensive investigations at a nano-scale.

In this paper, we present AFM observations of the effect of CO_3^{2-} ions on barite $\{001\}$ and $\{210\}$ surfaces, while growing from aqueous solutions with a given supersaturation with respect to barite. Two different series of AFM experiments were conducted: (i) runs where the aim was to determine the carbonate concentration needed to inhibit growth on the barite $\{001\}$ and $\{210\}$ faces; (ii) runs where the aim was to determine the supersaturation that leads to the recovery of growth out of the dead zone. Special attention has been paid to the growth behaviour of the first monolayers.

2. Experimental procedure

2.1. Inhibition experiments

In situ AFM experiments were carried out to study the changes in both the microtopography and the growth kinetics occurring on barite $\{001\}$ and $\{210\}$ surfaces when they grow from aqueous solutions bearing carbonate. For this purpose, natural barite crystals (León, Spain) were cleaved along the mentioned surfaces and placed inside the fluid cell of a Digital Instruments Multimode AFM. Then, supersaturated BaSO_4 solutions with different carbonate concentrations were passed over the surfaces. Images were taken during the whole growth process. Special attention

was paid to changes in the morphology of monomolecular steps and two-dimensional islands. In addition, systematic measurements of the growth rates of islands spreading on both the original barite substrate and the subsequent layers were taken on the $\{001\}$ and $\{210\}$ faces. Tables 1 and 2 show the concentrations of BaCl_2 , Na_2SO_4 and Na_2CO_3 , the pH values and the supersaturations with respect to barite of the aqueous solutions used in the inhibition experiments. The concentrations of barium and sulphate were maintained constant, while the carbonate ion concentration was varied. The activities of the different chemical species were calculated using PHREEQC [21]. The supersaturations with respect to barite were calculated using the following expression: $\beta_{\text{barite}} = a(\text{Ba}^{2+}) \cdot a(\text{SO}_4^{2-}) / K_{\text{sp,barite}}$ (where $a(\text{Ba}^{2+})$ and $a(\text{SO}_4^{2-})$ are the activities of the free ions in the solution and $K_{\text{sp,barite}}$ is the solubility product for barite = $10^{-9.98}$ at 25°C [22]). In all the experiments the supersaturation with respect to barite was approximately 12 for experiments on $\{001\}$ faces and 7 for experiments on $\{210\}$ faces, sufficiently high to ensure

Table 1

Concentrations, pH and supersaturation with respect to barite of the aqueous solutions used in inhibition experiments conducted on barite $\{001\}$ faces

Solution composition (mM)			pH	Supersaturation β_{barite}
BaCl_2	Na_2SO_4	Na_2CO_3		
0.04	0.04	0	7	12.59
0.04	0.04	0.01	8.9	12.59
0.04	0.04	0.02	9.2	12.30
0.04	0.04	0.03	9.4	12.30
0.04	0.04	0.04	9.5	12.30
0.04	0.04	0.05	9.6	12.02
0.04	0.04	0.06	9.6	12.02
0.04	0.04	0.07	9.7	12.02
0.04	0.04	0.08	9.7	12.02
0.04	0.04	0.09	9.8	11.74
0.04	0.04	0.1	9.8	11.74
0.04	0.04	0.11	9.9	11.75
0.04	0.04	0.15	9.98	11.48
0.04	0.04	0.2	10.1	10.96

Table 2

Concentrations, pH and supersaturation with respect to barite of the aqueous solutions used in the inhibition experiments conducted on barite $\{210\}$ faces

Solution composition (mM)			pH	Supersaturation β_{barite}
BaCl_2	Na_2SO_4	Na_2CO_3		
0.03	0.03	0	7	7.24
0.03	0.03	0.001	8	7.24
0.03	0.03	0.003	8.47	7.24
0.03	0.03	0.005	8.68	7.24
0.03	0.03	0.01	8.97	7.24
0.03	0.03	0.02	9.25	7.08
0.03	0.03	0.03	9.41	7.08
0.03	0.03	0.04	9.52	7.08
0.03	0.03	0.05	9.60	6.92
0.03	0.03	0.06	9.68	6.92

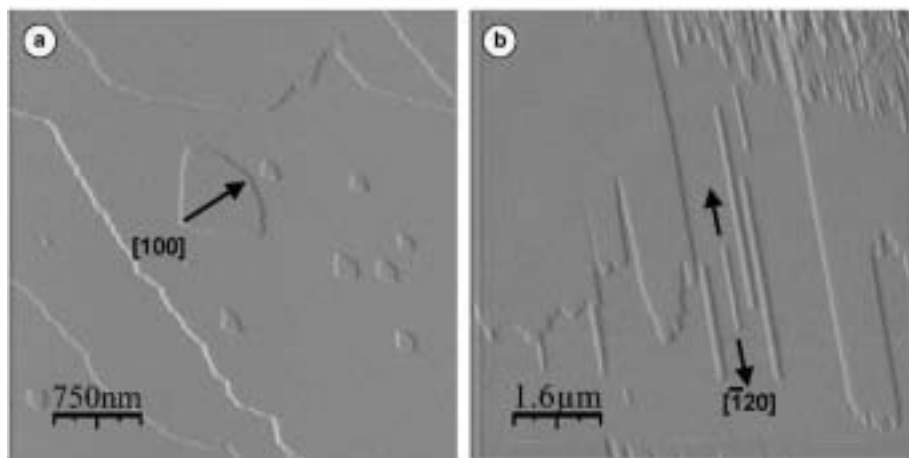


Fig. 1. AFM images of two-dimensional islands on barite surfaces. (a) Circular sector shape two-dimensional islands growing on a $\{001\}$ face. Growth rates were measured along the $[100]$ direction. (b) Needle-shape two-dimensional islands growing on a $\{210\}$ face. Growth rates were measured along the $[120]$ direction.

the formation of two-dimensional islands on these faces. The two-dimensional islands formed on each face have a distinctive shape: while those growing on $\{001\}$ faces are circular sector-shaped, on $\{210\}$ faces are needle-shaped (see Fig. 1).

For all the solutions used, the supersaturation with respect to witherite was calculated using the expression: $\beta_{\text{witherite}} = a(\text{Ba}^{2+}) \cdot a(\text{CO}_3^{2-}) / K_{\text{sp,witherite}}$ (where $a(\text{Ba}^{2+})$ and $a(\text{CO}_3^{2-})$ are the activities of the free ions in the solution and $K_{\text{sp,witherite}}$ is the solubility product for witherite = $10^{-8.56}$ at 25 °C [23]). In all the cases, its value was lower than 1, which means that the crystallization of witherite can be discarded. In order to maintain supersaturation constant, fresh solution was injected at intervals of about 1 min between each AFM scan. All the AFM images shown in this paper were taken in constant force mode while displaying the cantilever deflection signal. Height images were also taken in order to determine the thickness of monolayers. For each experiment several measurements of growth rates of two-dimensional islands have been carried out. In the experiments on the barite $\{001\}$ faces, growth rates were measured along the $\langle 100 \rangle$ directions of the two-dimensional islands. In the case of $\{210\}$ faces, growth rates were measured along the $\langle 120 \rangle$ directions of the two-dimensional islands (see Fig. 1).

2.2. Recovery experiments

A series of experiments were carried out in order to observe the recovery of growth on barite $\{001\}$ and $\{210\}$ faces previously inhibited. Normally, growth recovery requires a considerable increase in the supersaturation of the growth medium. In the case that we are dealing with, each face shows a distinctive behaviour. To make these differences obvious we carried out the recovery experiments in two parts: (i) Solutions supersaturated with respect to barite and containing carbonate were passed over freshly cleaved barite $\{001\}$ faces. The carbonate concentrations

in the solutions were high enough to promote the complete inhibition of growth after the formation of the second layer: 0.2 and 0.3 mM for barite $\{001\}$ and 0.05 mM for barite $\{210\}$ faces. (ii) Carbonate-free aqueous solutions with increasing supersaturation with respect to barite were passed over barite surfaces previously inhibited. This allowed us to determine the supersaturation level required to recover growth on each face.

3. Inhibition of growth on barite $\{001\}$ and $\{210\}$ surfaces

3.1. Barite $\{001\}$ face

When an aqueous solution with $[\text{Ba}^{2+}] = [\text{SO}_4^{2-}] = 0.04$ mM ($\beta_{\text{barite}} = 12.6$) is passed over a freshly cleaved barite $\{001\}$ face, two-dimensional nucleation is rapidly promoted. The nucleation on barite $\{001\}$ surface was previously described [24]. Two-dimensional islands are half-unit cell high and show a characteristic circular sector shape with straight edges parallel to $\langle 120 \rangle$ directions. The orientation of the islands is rotated 180° in successive layers. Both the nucleation and the spreading of two-dimensional islands on barite $\{001\}$ surfaces also occur in the presence of different amounts of CO_3^{2-} ions. Fig. 2a shows two-dimensional islands growing on a barite $\{001\}$ face from a supersaturated solution ($\beta_{\text{barite}} = 12.6$). After a few minutes, a solution with the same barium and sulphate concentration, but bearing carbonate, was passed over that surface (Fig. 2b–f). Although the two-dimensional islands continue growing, the presence of carbonate in the solution strongly modifies their growth kinetics. Table 3 shows the islands' growth rate (measured along the $[100]$ direction) on barite $\{001\}$ surfaces when supersaturated solutions contain increasing amounts of carbonate. In Fig. 3 the growth rates of two-dimensional islands versus the concentration of carbonate in the aqueous solution have been plotted. As can be seen, for aqueous solutions with carbonate concentrations below

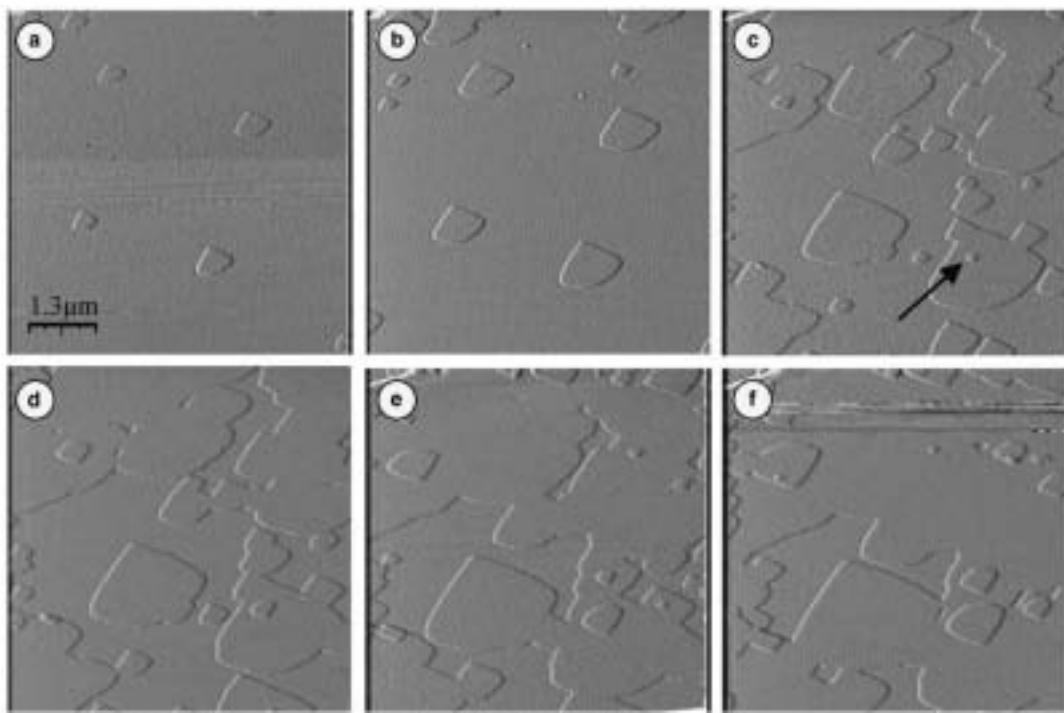


Fig. 2. Growth sequence observed on a barite {001} face from solutions of composition $[Ba^{2+}] = [SO_4^{2-}] = 0.04$ mM, in the absence and in the presence of carbonate. (a) Two-dimensional islands growing from a pure barium sulphate solution. (b-f) Growth from a solution with the same concentration of Ba^{2+} and SO_4^{2-} as in (a) but with 0.04 mM of CO_3^{2-} . Two-dimensional islands continue their growth while new islands form on the original barite substrate. Finally, a second generation of islands begins to grow. The island indicated with an arrow initially grows on the area previously grown in the absence of carbonate (c-e) and continue growing on areas that already had grown in the presence of carbonate (f). Growth sequence around 45 min.

Table 3
Carbonate concentrations and growth rates obtained in the inhibition experiments for barite {001} faces

Total carbonate (mM)	Growth rates (nm/s)		
	1st layer original substrate	2nd layer pure barite	2nd layer barite with carbonate
0.01	0.54	0.54	0.54
0.02	0.54	0.54	0.54
0.03	0.54	0.54	0.53
0.04	0.54	0.54	0.53
0.05	0.54	0.54	0.48
0.06	0.54	0.52	0.43
0.07	0.55	0.53	0.40
0.08	0.58	0.55	0.38
0.09	0.60	0.56	0.36
0.1	0.64	0.62	0.31
0.11	0.66	0.63	0.27
0.15	0.69	0.66	0.14
0.2	0.75	0.71	0

0.06 mM, the islands' growth rate on the original barite substrate remains constant, with a value of 0.54 nm/s. For higher carbonate concentrations, their growth rate increases with the concentration of carbonate, reaching a value of 0.75 nm/s for a carbonate concentration of 0.2 mM.

The growth kinetics of a second generation of islands (i.e. islands growing on the previously formed layer) depends on the region of the surface where they grow. Those

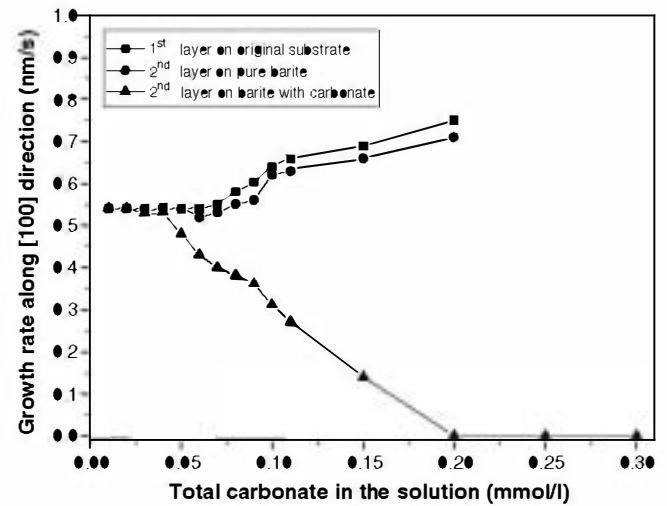


Fig. 3. Growth rates of two-dimensional islands spreading on barite {001} surfaces versus the total carbonate concentration in the aqueous solution. Growth rates were always measured along $\langle 100 \rangle$ direction. Solid squares correspond to the growth rates of two-dimensional islands that grew on original barite substrate. The solid circles represent the growth rates of the second generation of island that grew on areas previously grown in the absence of carbonate (inner part of the first generation of two-dimensional islands). Finally, solid triangles represent the growth rates of the second generation of two-dimensional islands when they spread on areas previously grown in the presence of carbonate.

islands which spread on the area formed before introducing carbonate (i.e. on top of the inner part of the two-dimen-

sional islands) maintain a constant rate of 0.54 nm/s for carbonate concentrations up to 0.06 mM. However, when higher carbonate concentrations are used, growth rates progressively increase, reaching a value of 0.71 nm/s for a carbonate concentration of 0.2 mM. This behaviour is identical to that observed when the first islands grew on the original pure barite (001) substrate. In Fig. 3, the small difference between the points corresponding to the growth rates measured for the first layer spreading on the original barite substrate (solid squares) and for the second layer spreading on pure barite (solid circles) is due to the difficulty of distinguishing the limit between the area of the first layer grown before and after injecting the carbonate-bearing solution. For carbonate concentrations higher than 0.2 mM, growth rate measurements were impossible due to the extremely high two-dimensional nucleation rate.

When islands of the second generation reach an area of the first layer grown from a solution containing carbonate, their growth rate decreases (solid triangles in Fig. 3). Such a decrease depends on the carbonate concentration. For a carbonate concentration below 0.04 mM, growth rates remain almost constant, with a value of 0.54 nm/s, i.e. the value corresponding to a pure BaSO₄ solution with a supersaturation $\beta_{\text{barite}} = 12.6$. However, for a carbonate concentration in the range from 0.04 to 0.2 mM, the islands growth rate decreases linearly as the carbonate concentra-

tion in the solution increases. For concentrations higher than 0.2 mM the growth is completely inhibited after the formation of the first monolayer of islands. These islands only grow either on the original barite substrate or on those regions of the first layer previously grown in the absence of carbonate. As a result, an exact reproduction of the nanotopography underneath is observed (see Fig. 4a–d). In contrast, when solutions with carbonate concentrations below 0.2 mM were used, successive monolayers formed.

Frequently, in the deflection images the boundary between areas grown in the absence and in the presence of carbonate appears as a line with a stronger contrast. This can clearly be observed in Fig. 5. By looking at the height AFM images it is obvious that monolayers grown incorporating carbonate are lower than pure barite monolayers. The amount of CO₃²⁻ incorporated must be significant since both deflection and height AFM images of the first CO₃²⁻-bearing monolayers show a homogeneous contrast. By considering the radius of curvature of the AFM tips used, we can roughly estimate a maximum distance between carbonates incorporated into barite (001) monolayers of 60 nm. Systematic measurements of the barite {001} monolayers height have been carried out on the AFM images. The results are shown in Table 4. In Fig. 6, the heights of the two-dimensional islands versus the concentration

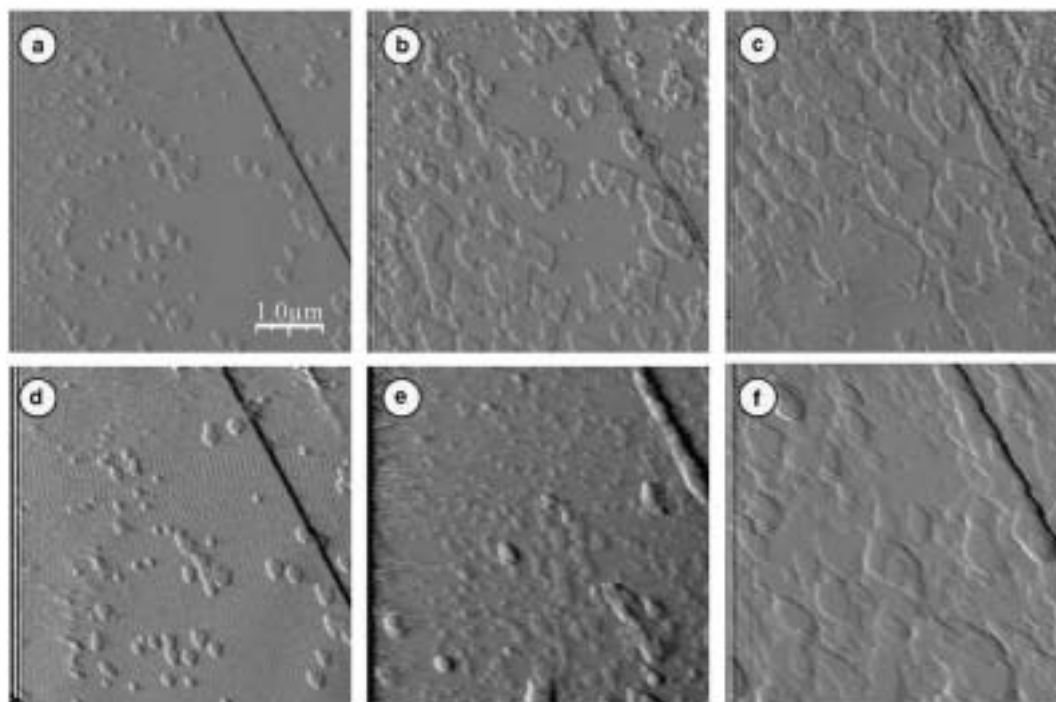


Fig. 4. Inhibition and recovery sequence on a barite (001) face from a solution of composition $[\text{Ba}^{2+}] = [\text{SO}_4^{2-}] = 0.04 \text{ mM}$ and $[\text{CO}_3^{2-}] = 0.2 \text{ mM}$. (a) First generation of two-dimensional islands previously grown in the absence of carbonate. (b, d) A solution supersaturated with respect to barite and containing carbonate is injected. The islands grow now incorporating carbonate and the islands on the original pure barite substrate coalesce and complete a monolayer ($\sim 3.5 \text{ \AA}$). (c, e) On the areas previously grown in the absence of carbonate (two-dimensional islands in (a)) the formation of a new generation of islands can be observed. These islands are not able to spread over areas previously grown in the presence of carbonate and the growth on the surface is inhibited. As a result, the original nanotopography is almost perfectly reproduced one monolayer higher (compare (a) and (d)). (f) A solution supersaturated with respect to barite ($\beta_{\text{barite}} = 31.6$) and without carbonate is injected. (e and f) The recovery of growth is observed.

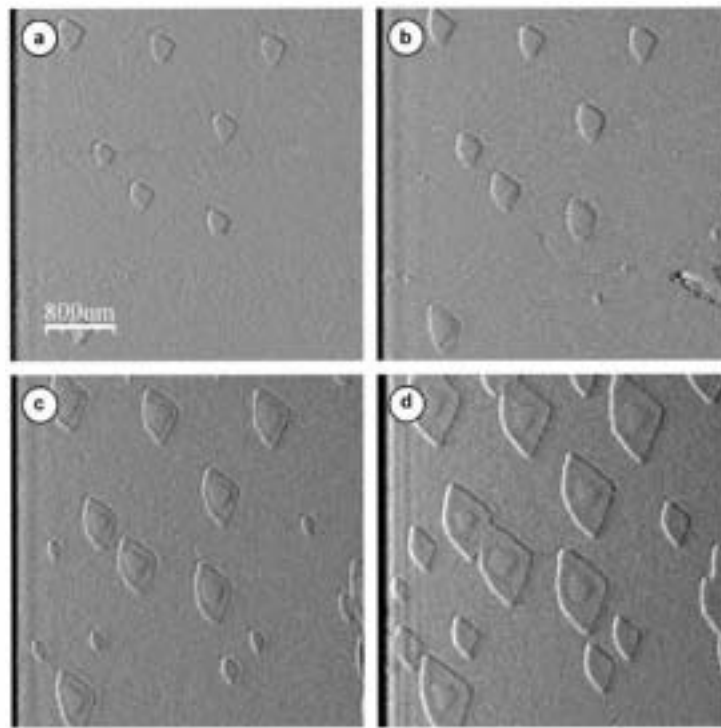


Fig. 5. Growth sequence taken during the growth of a barite (001) face when a solution with 0.2 mM of carbonate is injected. The AFM images show the formation of a layer with a different contrast around the islands previously formed without carbonate.

Table 4
Carbonate concentrations and height of the two-dimensional islands obtained in the inhibition experiments for barite {001} faces

Total carbonate (mM)	Height measurements (Å)
0.2	2.48
0.15	2.64
0.13	2.88
0.09	3.08
0.08	3.26
0.06	3.43
0.04	3.53
0.03	3.5
0.02	3.53
0.01	3.5
0	3.5

of carbonate in the aqueous solution have been plotted. As can be seen, for carbonate concentrations below 0.05 mM, two-dimensional islands show a constant height. However, when carbonate concentrations in the growth solutions are above 0.05 mM, the height of the islands clearly decreases.

3.2. Barite {210} face

The inhibition of growth on the barite {210} faces induced by the presence of CO_3^{2-} ions in the solution is similar to that observed on the {001} faces. In the absence of carbonate, when BaSO_4 solutions with a supersaturation with respect to barite of $\beta_{\text{barite}} = 7.2$ are passed over {210} surfaces, two-dimensional nucleation is rapidly promoted. Two-dimensional islands have one unit cell in

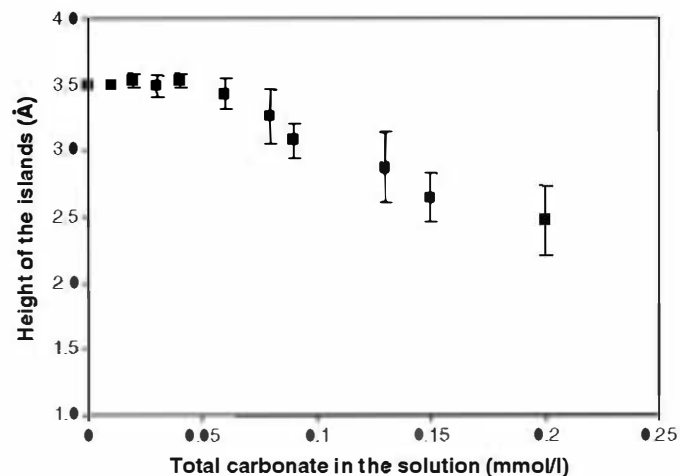


Fig. 6. Heights of the (001) two-dimensional islands versus the total carbonate concentration in the aqueous solution. Standard deviation error bars have also been plotted. The height of a pure barite monolayer is 3.5 Å.

height and a characteristic needle-shape, being their longest axis parallel to $\langle 120 \rangle$ directions. The growth of the islands on {210} faces is highly anisotropic: they grow very fast along one sense of the $[\bar{1}20]$ and very slow along the opposite sense of such a direction [25]. For the mentioned supersaturation, the measured growth rate along the $[\bar{1}20]$ is 3.7 nm/s. As in the case of {001} faces, the use of aqueous solutions with the same concentration of barium and sulphate, but bearing moderate amounts of carbonate, neither inhibits the nucleation nor the spreading of two-dimen-

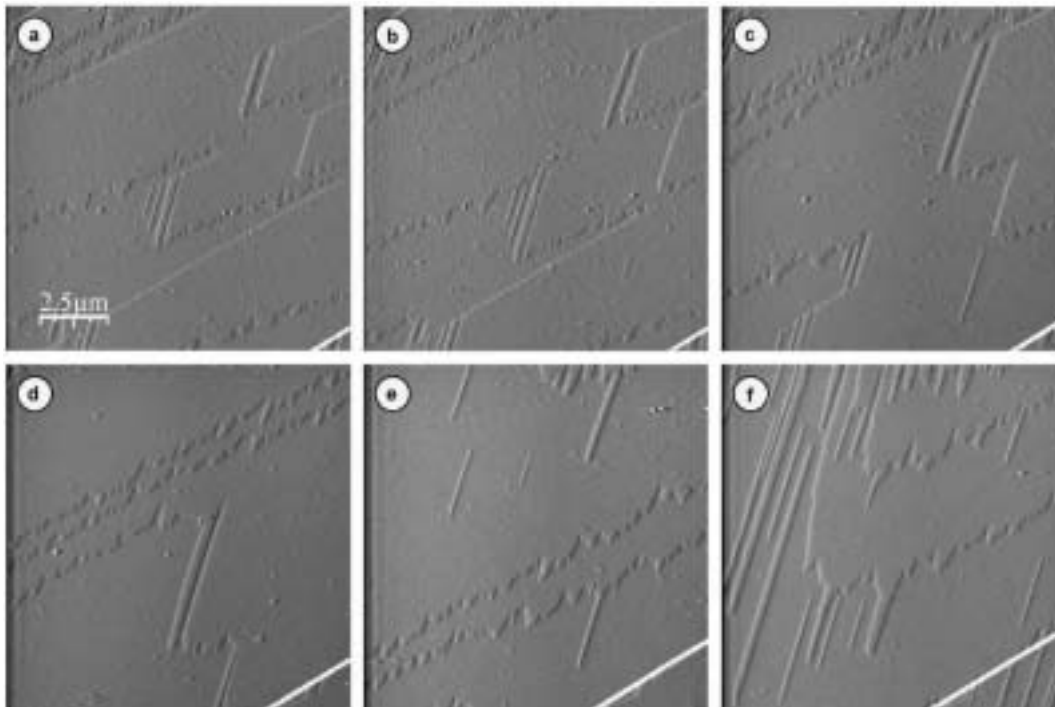


Fig. 7. Growth sequence on a barite {210} face from solutions of composition $[Ba^{2+}] = [SO_4^{2-}] = 0.03$ mM, in the absence and in the presence of carbonate. (a) Two-dimensional islands growing from a pure $BaSO_4$ solution. (b) Growth from a solution with the same concentration of Ba and SO_4 as in (a) but with 0.005 mM of CO_3^{2-} . This concentration of carbonate it is not high enough to inhibit the growth process after the formation of the first monolayer. Therefore, nucleation and spreading of two-dimensional layers occurs in successive layers.

sional islands on the original {210} surfaces. Fig. 7 shows a typical growth sequence on a barite {210} face. Two-dimensional islands initially grew from a supersaturated solution with respect to barite and in the absence of carbonate. A few minutes later, a solution with the same concentration of barium and sulphate, but bearing carbonate, was injected in the fluid cell of the AFM.

Although, the presence of carbonate in the growth solution does not modify the nanotopography of the surface, the growth rates of islands on successive layers again depend on the carbonate concentration. Table 5 and Fig. 8 show the growth rates along $\langle 120 \rangle$ directions as a function of the carbonate concentration in the aqueous solution.

Table 5
Carbonate concentrations and growth rates obtained in the inhibition experiments for barite {210} faces

Total carbonate (mM)	Growth rates (nm/s)	
	2nd layer pure barite	2nd layer barite with carbonate
0.001	3.7	3.7
0.003	3.7	3.7
0.005	3.7	3.7
0.01	4.2	3.2
0.02	4.64	2.8
0.03	5.1	1.8
0.04	5.5	0.5
0.05	5.7	0
0.06	6	0

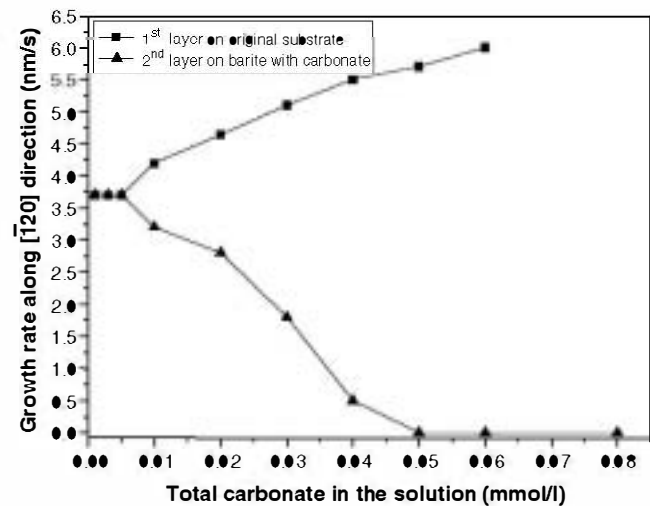


Fig. 8. Growth rates of two-dimensional islands on barite {210} faces versus the total carbonate concentration in the aqueous solution. Growth rates were always measured along the $[120]$ direction. Growth rates of two-dimensional islands that grew on original barite substrate have been plotted as solid squares; growth rates of the second generation of two-dimensional islands on areas previously grown in the presence of carbonate have been plotted as solid triangles. Measurements made on the second generation of islands that grew on areas previously grown in the absence of carbonate (inner part of the first generation of two-dimensional islands) coincide with the solid squares and they have not been plotted.

When solutions with low carbonate concentrations (from 0.001 to 0.005 mM) are placed in contact with barite

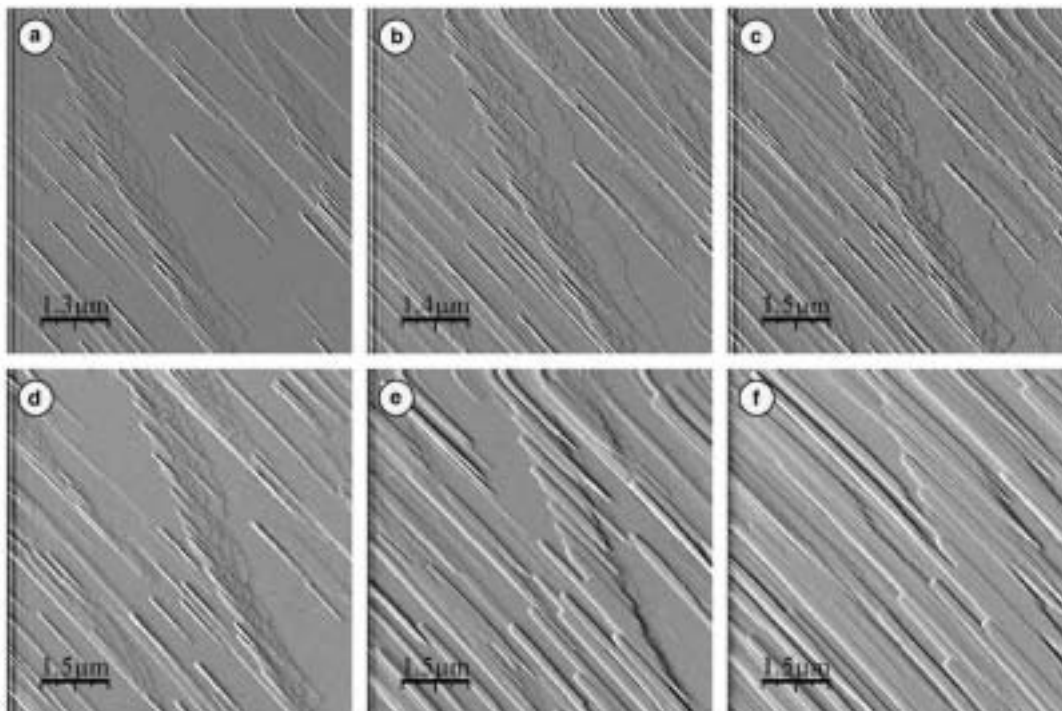


Fig. 9. Inhibition and recovery sequence on a barite (210) face from a solution of composition $[\text{Ba}^{2+}] = [\text{SO}_4^{2-}] = 0.03 \text{ mM}$ and $[\text{CO}_3^{2-}] = 0.05 \text{ mM}$. (a) First generation of two-dimensional islands previously grown in the absence of carbonate. (b-d) The growth is inhibited after injecting a solution supersaturated with respect to barite and containing carbonate. The original nanotopography is almost perfectly reproduced one monolayer higher (compare (a) and (d)). (d) A solution supersaturated with respect to barite ($p_{\text{barite}} = 7.2$) and without carbonate is injected. (e and f) The recovery of growth is observed.

{210} faces, the first generation of islands spreads on the original (210) substrate at a constant rate of 3.7 nm/s, i.e. the same rate as in the absence of carbonate. However, for carbonate concentrations higher than 0.005 mM, the growth rates of this first generation of islands increase with the concentration of carbonate in the solution (solid squares in Fig. 8). Thus, for a carbonate concentration of 0.06 mM the islands growth rate measured along the {120} directions is 6 nm/s.

The growth kinetics of the second generation of islands (i.e. islands formed on the previously grown first layer) again depends on what area of the first layer they grow. Those islands spreading on areas previously grown either in the absence of carbonate or from solutions with carbonate concentrations below 0.005 mM, grow at a constant rate of 3.7 nm/s. For carbonate concentrations higher than 0.005 mM, growth rates increase with the carbonate concentration in the same way as occurred with the two-dimensional islands on the original barite (210) substrate. In this case, growth rate measurements exactly coincide with those obtained for the islands growing on the original substrate (solid squares in Fig. 8). However, when islands corresponding to the second generation reach areas previously grown in the presence of carbonate, growth rates behaviour depends on the carbonate concentration in the aqueous solution. Thus, for carbonate concentrations below 0.005 mM growth rates remain almost constant, with a value of 3.7 nm/s, while for carbonate concentrations in

the range from 0.005 to 0.05 mM growth rates decrease linearly as the carbonate concentration in the aqueous solution increases. Finally, for carbonate concentrations above 0.05 mM the growth of the second generation of islands is completely inhibited. In this case, again the nanotopography underneath is exactly reproduced (see Fig. 9a-d).

4. Recovery of barite {001} and {210} faces from “dead zone”

In the next subsections we will describe the results of a series of experiments conducted to determine under which conditions growth on {001} and {210} surfaces recovers after it has been completely inhibited by the presence of carbonate in the growth solution. For this purpose, aqueous solutions with different supersaturation levels with respect to barite have been passed over previously inhibited barite surfaces. Our AFM observations show that, for the time-scale considered, the behaviour of growth recovery on barite {001} and {210} surfaces differs.

4.1. Barite {001} faces

As has been described in Section 3.1, for aqueous solutions with $[\text{Ba}^{2+}] = [\text{SO}_4^{2-}] = 0.04 \text{ mM}$, growth on barite {001} surfaces is totally inhibited when the solution contains carbonate concentrations higher than 0.2 mM. The

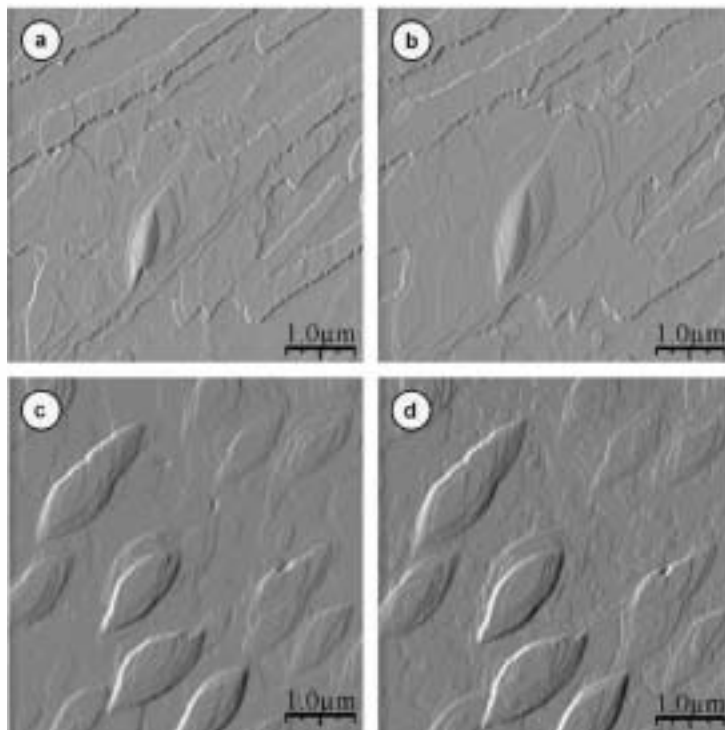


Fig. 10. Spirals formed during the recovery of growth on a barite {001} surface previously inhibited using a solution of composition $[\text{Ba}^{2+}] = [\text{SO}_4^{2-}] = 0.04 \text{ mM}$ and $[\text{CO}_3^{2-}] = 0.3 \text{ mM}$. The composition of the solution used to recover the growth on the surface was $[\text{Ba}^{2+}] = [\text{SO}_4^{2-}] = 0.07 \text{ mM}$ (supersaturation with respect to barite $\beta_{\text{barite}} = 36.3$).

total inhibition occurs after the formation of a single monolayer that covers (and reproduces) the original nanotopography. In order to recover the growth on this surface, it is necessary to increase the supersaturation of the solution with respect to barite. We conducted recovery experiments by passing pure BaSO_4 aqueous solutions with increasing supersaturations over the previously inhibited barite {001} surfaces.

As has been explained above, the growth inhibition also leads to the almost perfect reproduction of the original nanotopography (compare for example Fig. 4d with Fig. 4a). Experiments using solutions with different supersaturations with respect to barite showed that no recovery of growth occurred when the supersaturation value was smaller than 31.6, although the surface was maintained in contact with the solutions for a period of time longer than 750 s. However, for solutions with a $\beta_{\text{barite}} \geq 31.6$, a few seconds after injecting the solution, the recovery of growth on barite {001} faces occurs (Fig. 4e and f). Initially, the shape of two-dimensional islands forming on the surface differs from the characteristic circular sector. However, as growth proceeds and successive layers are formed, the circular sector shape of the islands is also recovered.

Recovery of growth have been also observed on barite {001} surfaces previously inhibited after growing from solutions with composition $[\text{Ba}^{2+}] = [\text{SO}_4^{2-}] = 0.04 \text{ mM}$ and $[\text{CO}_3^{2-}] = 0.3 \text{ mM}$. In this case, a higher supersaturation with respect to barite ($\beta_{\text{barite}} = 36.3$) was needed to recover growth. Moreover, during the recovery process,

numerous growth spirals formed on areas of the surface where no screw dislocations existed previously (see Fig. 10). This implies that there is a relationship between the incorporation of carbonate ions into {001} surface and the formation of screw dislocations. Since the development of such growth spirals has been observed in a number of independent experiments, it seems to be a typical feature of the recovery of barite {001} surfaces inhibited after growing from solutions bearing high amounts of carbonate.

4.2. Barite {210} faces

The behaviour of the recovery of growth on barite {210} faces substantially differs from that observed on {001} faces. Growth on {210} faces previously inhibited by carbonate spontaneously starts to recover after a short period of time ($\sim 750 \text{ s}$) in contact with carbonate-free solutions with the same BaSO_4 concentration as the initial growth solution. Fig. 9a–d show the inhibition of a barite (210) surface using a solution with composition $[\text{Ba}^{2+}] = [\text{SO}_4^{2-}] = 0.03 \text{ mM}$ and $[\text{CO}_3^{2-}] = 0.05 \text{ mM}$. The growth recovers when a carbonate-free solution with composition $[\text{Ba}^{2+}] = [\text{SO}_4^{2-}] = 0.03 \text{ mM}$ is passed over the surface (Fig. 9e–f). Fig. 11 shows the growth rate evolution during the recovery process on a barite (210) face. As can be seen, during the first minutes after injecting the “recovering” solution, the (210) surface does not grow. However, after about 10 min, two-dimensional islands start to grow and,

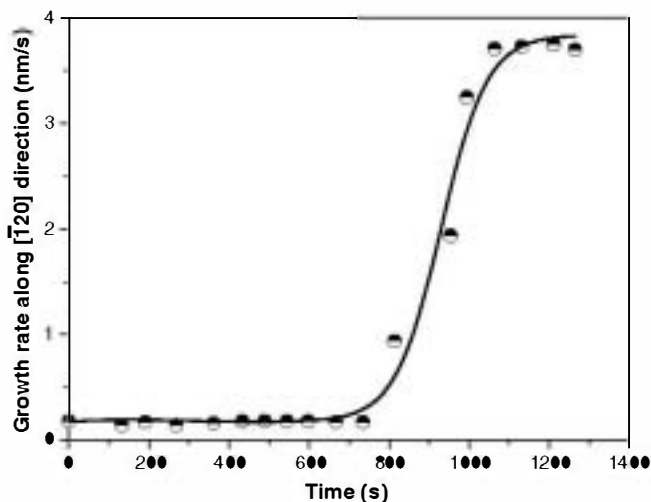


Fig. 11. Recovery growth rates of the two-dimensional islands on {210}. Growth rates were always measured along the $[120]$ direction.

rapidly, a growth rate of 3.7 nm/s is reached. This growth rate coincides with that measured when a solution with identical composition was passed over the original pure barite substrate. Once the surface is recovered, growth proceeds normally and successive layers show no signs of defect formation, in contrast with what has been observed on {001} surfaces.

5. Discussion

5.1. Inhibition of growth on barite {001} and {210} faces by CO_3^{2-} ions

AFM observations presented in Section 3 demonstrate that the presence of CO_3^{2-} ions in the growth solutions strongly inhibits continuous layer-by-layer growth on barite {001} and {210} faces. In the case of barite {001} faces, such an inhibition is accompanied by a clear decrease in the height of the two-dimensional island. Our measurements show that for carbonate concentrations below 0.05 mM (i.e. carbonate concentration for which no growth inhibition is detected) the height of the two-dimensional islands remains constant, with a value of 3.5 Å (the height of the elementary growth layer for pure barite {001} faces [26]). However, above the threshold carbonate concentration ($[\text{CO}_3^{2-}] = 0.05$ mM), inhibition occurs and simultaneously the height of {001} two-dimensional islands decreases with the carbonate concentration in the aqueous solution (Fig. 6). The height of the islands grown from a solution containing 0.2 mM is 2.48 Å, which means a 30% decrease compared to the height of a pure barite monolayer. This result is consistent with a certain degree of substitution of the large SO_4^{2-} tetrahedral groups by the smaller CO_3^{2-} triangular groups in the barite structure. Therefore, we can conclude that during the growth of barite {001} faces from solutions bearing carbonate, CO_3^{2-} groups incorporate into barite structure.

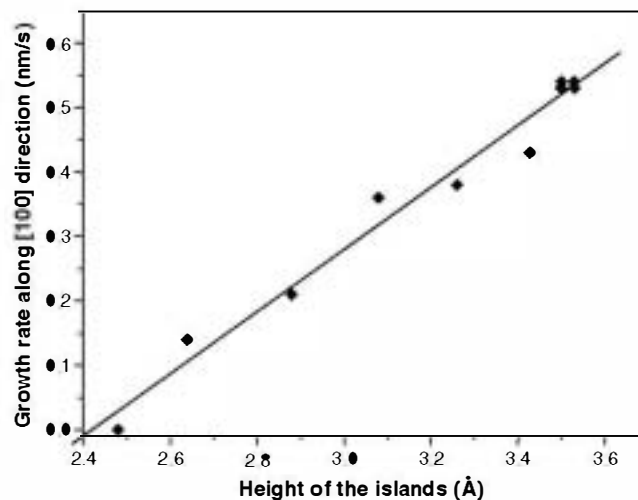


Fig. 12. Growth rate of the second generation of two-dimensional islands on barite {001} face along $[100]$ direction versus two-dimensional islands height. Data fit well to a linear function (correlation coefficient $R = 0.99$).

On barite {001} faces, the incorporation of CO_3^{2-} in the first monolayer seems to be energetically favourable since two-dimensional islands grow at higher velocity as the carbonate concentration increases in the aqueous solution. The incorporation of carbonate in this first monolayer determines the subsequent growth inhibition. When the second generation of islands starts to grow on areas that had incorporated CO_3^{2-} , growth rates decrease linearly with the carbonate concentration until the growth is completely inhibited for $[\text{CO}_3^{2-}] = 0.2$ mM. Fig. 12 shows the relationship between the height of the second generation of two-dimensional islands and their growth rate along $[100]$ direction. As can be seen, the rate of spread on the surface linearly decreases with the decrease of height of the islands. As the height of the island is an indirect measurement of the degree of substitution of SO_4^{2-} anions by CO_3^{2-} groups (the higher the substitution the smaller the height), it can be concluded that the incorporation of CO_3^{2-} in barite {001} surfaces leads to a clear decrease of the growth rate on this surface. The growth inhibition must be related to changes in barite {001} surfaces properties induced by CO_3^{2-} incorporation (e.g. slight distortion of bond lengths, number of kink positions, etc.). Furthermore, the differences in height between the original barite terraces and the first monolayer incorporating carbonate result in the formation of sub-nanosteps. Such sub-nanosteps can constitute an actual physical barrier for the advancement of subsequent monolayers. However, a complete understanding of the role played by CO_3^{2-} anions during the inhibition of barite {001} faces growth will require a more detailed investigation using other surface sensitive techniques (e.g. XPS, TOF-SIMS), which is beyond the scope of this work.

The growth of barite {210} faces is much more strongly affected by the presence of carbonate in the aqueous solution. Thus, the carbonate concentration required to promote the complete inhibition of the second monolayer growth in the case of {210} faces is 4 times

lower ($[\text{CO}_3^{2-}] = 0.05 \text{ mM}$) than in the case of $\{001\}$ faces ($[\text{CO}_3^{2-}] = 0.2 \text{ mM}$). If inhibition of growth on $\{210\}$ surface results from the incorporation of CO_3^{2-} into barite monolayers, this must be very limited. No decrease of the height of the two-dimensional monolayers growing in the presence of carbonate has been measured on $\{210\}$ surfaces. This is consistent with such a limited incorporation, although it could also mean that in this case growth inhibition results from the adsorption of CO_3^{2-} on specific points of the two-dimensional islands, without incorporating into the structure. However, since the growth of the first monolayer in the presence of CO_3^{2-} is faster than in its absence, incorporation seems to be a more likely mechanism.

The much higher sensitivity of barite $\{210\}$ surfaces to the presence of carbonate anions in the growth medium can be explained if we considered the different geometry of two-dimensional island on $\{210\}$ and $\{001\}$ surfaces. As has been explained above, two-dimensional islands on $\{210\}$ are highly anisotropic, with an elongated shape and a faster growth rate along one sense of the $\langle 120 \rangle$ directions. It is evident that a small number of CO_3^{2-} anions either incorporating in or adsorbing on the ends of the elongated two-dimensional islands will be able to completely stop the growth on $\{210\}$ surfaces. On the contrary, two-dimensional islands on $\{001\}$ are circular sector-shaped, with straight edges parallel to $\langle 120 \rangle$ directions. In this case, growth mainly occurs by the advancement of the large curved edge, which has a higher number of kink-sites than the narrow edge of two-dimensional islands on $\{210\}$ [25,27]. Therefore, to completely inhibit growth on $\{001\}$ faces a high number of CO_3^{2-} anions has to incorporate into the kink-sites of the curved edge of the two-dimensional islands.

Our observations of growth in the presence of carbonate on both barite $\{001\}$ and $\{210\}$ faces show that the kinetics of advancement of the first and the subsequent monolayers is completely different. While the effect of carbonate on the first monolayer consists in increasing its rate of spreading, a clear reduction of the growth rate of the successive monolayers is observed. Although the general behaviour of the growth inhibition on barite $\{001\}$ and $\{210\}$ surfaces can be explained by the classical “isomorphic incorporation” model i.e. the growth rate decrease as the concentration of carbonate in the aqueous solution increases, the behaviour of the first monolayer is difficult to interpret on the basis of this model. A similar behaviour of the first monolayer has been observed in other systems [17,19]. This indicates that during the growth of crystalline faces from multicomponent aqueous solutions the formation of a faster first monolayer plays an important and poorly understood role.

5.2. Recovery of growth on barite $\{001\}$ and $\{210\}$ faces

Although barite $\{001\}$ and $\{210\}$ faces exhibit a similar growth inhibition behaviour in the presence of carbonate, the recovery of growth (i.e. the exit from the so-called dead

zone) is different on each face. Thus, once growth inhibition has occurred, in order to recover the growth on barite $\{001\}$ faces it is necessary to considerably increase the supersaturation for barite of the carbonate-free aqueous solution. On the contrary, in the case of $\{210\}$ faces the growth recovery spontaneously occurs using a carbonate-free aqueous solution with the same concentration of sulphate and barium as the solution used in the inhibition experiment. This different recovery behaviour can be related to the different amount of carbonate previously required to completely inhibit growth on each barite face. As has been explained in Section 3, in the case of $\{001\}$ faces a minimum concentration of carbonate of 0.2 mM is needed to stop growth after the formation of the first barite monolayer. Such a monolayer contains a significant amount of carbonate and only free-carbonate aqueous solutions with a supersaturation $\beta_{\text{barite}} \geq 31.2$ are able to promote growth again on $\{001\}$ (although no recovery has been observed for solutions with $\beta_{\text{barite}} < 31.2$ during the time of the experiment, we cannot rule out the possibility that growth could recover after very long periods of time of exposure to such carbonate-free aqueous solutions). The recovery process starts on those regions of the surface where two-dimensional nucleation is easier, e.g. steps edges. After a few minutes, growth is observed on the whole surface, although with a non-homogeneous covering. Such an inhomogeneity of growth reflects that the substrate has an important degree of strain around the point defects, resulting from the extensive substitution of large SO_4^{2-} anions by small CO_3^{2-} groups. The existence of this substrate strained at nano-scale is more clearly evidenced when we study the recovery on barite $\{001\}$ surfaces previously inhibited using a solution with a higher concentration of carbonate ($[\text{CO}_3^{2-}] = 0.3 \text{ mM}$). After growth inhibition, a higher supersaturation ($\beta_{\text{barite}} = 36.3$) will also be required for recovery on this surface. In this case, the recovery of growth leads to the formation of numerous growth spirals on the surface. Since spiral growth necessarily implies the emergence of screw dislocations, we can conclude that $\{001\}$ faces grown in the presence of carbonate are highly defective. At present, we are not in conditions to propose a mechanism for the generation of screw dislocations. However, such generation must be related to the lattice stress associated to the inhomogeneous incorporation of CO_3^{2-} into the uppermost monolayer of barite $\{001\}$ surface, which can be substantially reduced by the formation of shallow screw dislocations.

The spontaneous recovery of growth on $\{210\}$ faces after a few seconds in contact with a carbonate-free aqueous solution with the same concentration of sulphate and barium as the solution used for the inhibition also has to be related to the very small amount of carbonate required to promote growth inhibition on this surface. As no difference in height between layers grown from solutions with and without carbonate has been measured, we cannot conclude whether inhibition is due to incorporation or adsorption of CO_3^{2-} groups on the ends of the elongated

two-dimensional islands. Depending on the inhibition mechanism (incorporation or adsorption of CO_3^{2-}), the recovery mechanism will be also different. If we assume incorporation as the inhibition mechanism, a nano-barrier will exist at the boundary between the first and the second monolayer. Such a nano-barrier would be very small and could easily be overcome. This is consistent with the existence of an induction time (about 730 s) before the inhibited two-dimensional islands start to grow again. Furthermore, once growth resumes on $\{210\}$ surfaces, there also exists an induction time for the nucleation of new generations of two-dimensional islands on such a surface. The existence of an induction time would also be consistent with the adsorption of CO_3^{2-} groups. In this case, after a short period of time in contact with a carbonate-free solution, the adsorbed CO_3^{2-} groups could abandon their position on the surface and pass to the solution. The release of CO_3^{2-} groups would leave barite $\{210\}$ surface free to grow again. However, the hypothesis of a simple adsorption of CO_3^{2-} is difficult to conciliate with the fact that the growth rate of the first monolayer increases, while the second monolayer grows slower. A definite explanation of both growth inhibition and recovery on $\{210\}$ will require further investigations.

6. Conclusion

AFM observations show that under moderate supersaturation conditions, the presence of carbonate in the aqueous solution inhibits the growth of barite $\{001\}$ and $\{210\}$ faces. A threshold concentration of carbonate in the aqueous solution is required to promote growth inhibition. This concentration is 4 times higher for $\{001\}$ than for $\{210\}$. In the case of $\{001\}$ faces, a high amount of carbonate is incorporated into the first monolayer. This is reflected by a decrease of the height of the two-dimensional islands growing on the face. The incorporation of carbonate into the barite structure changes the surface characteristics (e.g. distortion of bonds and formation of sub-nanosteps). In the case of $\{210\}$ faces, the inhibition effect of CO_3^{2-} ions is not accompanied by a measurable decrease in the height of the first monolayer. Therefore, it cannot be completely discarded that adsorption of CO_3^{2-} could play a role in the inhibition.

On both $\{001\}$ and $\{210\}$ faces, the second monolayers spread on the surfaces with rates inversely proportional to the carbonate concentration in the aqueous solution, the inhibition being complete above a certain carbonate concentration value. For a given supersaturation with respect to barite, this value is face-specific.

Recovery experiments conducted on previously inhibited surfaces show a different behaviour for $\{001\}$ and $\{210\}$. While growth recovery on $\{001\}$ faces requires to considerably increase the supersaturation for barite of a carbonate-free aqueous solution, it occurs spontaneously on $\{210\}$ when these faces are placed in contact with a carbonate-free solution with the same concentration of sul-

phate and barium as the solution used in the inhibition experiment.

The results presented here indicate that inhibition and recovery of growth phenomena on barite $\{001\}$ and $\{210\}$ faces are complex and they involve a number of distinctive processes. Of special interest is the different growth behaviour of the first monolayer compared to subsequent monolayers: the first monolayer always increases its growth rate in the presence of a carbonate concentration above the inhibition concentration threshold. In addition, the rapid spreading of a first carbonate-bearing monolayer determines the subsequent inhibition of growth on barite faces. This observation is in agreement with previous AFM observations of growth inhibition in other systems [17 and references therein, 19], indicating that the formation of a first monolayer during crystal growth inhibition strongly controls the effectiveness of incorporating ions as inhibitors. This fact seems to be an interesting starting point for a future improvement of the classical isomorphic impurity incorporation model.

Finally, the observed differences in the amount of carbonate required to inhibit growth on barite $\{001\}$ and $\{210\}$ faces, together with the different recovery behaviour of both faces, can be useful for interpreting typical barite morphologies found in natural environments (e.g. desert roses), as well as for obtaining information about barite genesis.

Acknowledgements

The authors thank Institut für Mineralogy Münster (Germany) for kindly providing them access to AFM. N. Sánchez-Pastor acknowledges financial support from Spanish Ministry of Education and Science (FPI grant). C.M. Pina and J.M. Astilleros acknowledge Spanish Ministry of Education and Science for financial support ("Ramón y Cajal" program). This work has been financially supported by Spanish Ministry of Education and Science (Project number: BTE2002-00325). The barite sample was kindly provided by Begoña Sánchez and Javier García-Guinea (Museo Nacional de Ciencias Naturales, Spain). Constructive criticism was provided by anonymous reviewers.

References

- [1] N. Cabrera, D.A. Vermilyea, in: R.H. Doremus, B.W. Roberts, D. Turnbull (Eds.), *Growth and Perfection of Crystals*, Chapman & Hall, London, 1958, p. 393.
- [2] K. Sangwal, I. Owczarek, *J. Cryst. Growth* 129 (1993) 640.
- [3] W.J.P. van Enckevort, C.J.F. van den Berg, K.B.G. Kreuwel, A.J. Derksen, M.S. Couto, *J. Cryst. Growth* 1 (1996) 156.
- [4] T.A. Land, T.L. Martin, S. Potapenko, G.T. Palmore, J.J. De Yoreo, *Nature* 399 (1999) 442.
- [5] R.J. Davey, J.W. Mullin, *J. Cryst. Growth* 23 (1974) 89.
- [6] I. Sunagawa, in: I. Sunagawa (Ed.), *Morphology of Crystals*, Terra Scientific Publishing Company (TERRAPUB), Tokyo, 1987, p. 509.
- [7] S. Mann, *Angew. Chem. Int. Ed.* 39 (2000) 3392.

- [8] D.P. Grigoriev, *Ontogeny of crystals*, Israel Program for Scientific Translations, Jerusalem, 1968, 250pp.
- [9] N. Kubota, J.W. Mullin, *J. Cryst. Growth* 152 (1995) 203.
- [10] Y. Yoshioka, T. Matsui, M. Kasuga, T. Irisawa, *J. Cryst. Growth* 198/199 (1999) 71.
- [11] R.A. Berner, *Geochim. Cosmochim. Acta* 39 (1975) 489.
- [12] W.J.P. van Enkevort, A.C.J.F. van den Berg, *J. Cryst. Growth* 183 (1998) 441.
- [13] K.J. Davies, P.M. Dove, J.J. De Yoreo, *Science* 290 (2000) 1134.
- [14] A.A. Chernov, *Modern Crystallography III (Crystal Growth)*, Springer Verlag, 1984, p. 517.
- [15] J.M. Astilleros, C.M. Pina, L. Fernández-Díaz, A. Putnis, *Geochim. Cosmochim. Acta* 66 (2002) 3177.
- [16] J.M. Astilleros, C.M. Pina, L. Fernández-Díaz, A. Putnis, *Chem. Geol.* 193 (2003) 93.
- [17] J.M. Astilleros, C.M. Pina, L. Fernández-Díaz, A. Putnis, *Surf. Sci.* 545 (2003) L767.
- [18] S.J. Freij, A. Putnis, J.M. Astilleros, *J. Cryst. Growth* 267 (2004) 288.
- [19] S.R. Higgins, X. Hu, *Geochim. Cosmochim. Acta* 69 (2005) 2085.
- [20] L.E. Wasylenki, P.M. Dove, D.S. Wilson, J.J. De Yoreo, *Geochim. Cosmochim. Acta* 69 (2005) 3017.
- [21] D.L. Parkhurst, C.A.J. Appelo, User's guide to PHREEQC (version 2). A computer program for speciation, batch-reaction, one-dimensional transport, and inverse geochemical calculations, US Geological Survey Water-Resources Investigations Report 99-4259, 2000, p. 312.
- [22] C.W. Blount, *Am. Miner.* 62 (1977) 942.
- [23] E. Busenberg, L.N. Plummer, *Geochim. Cosmochim. Acta*. 50 (1986) 2225.
- [24] C.M. Pina, D. Bosbach, M. Prieto, A. Putnis, *J. Cryst. Growth* 187 (1998) 119.
- [25] C.M. Pina, U. Becker, P. Risthaus, D. Bosbach, A. Putnis, *Nature* 395 (1998) 483.
- [26] P. Hartman, C.S. Strom, *J. Cryst. Growth* 97 (1989) 502.
- [27] S.R. Higgins, D. Bosbach, C.M. Eggleston, K.G. Knauss, *J. Phys. Chem. B* 104 (2000) 6978.